References and Notes

1. J. S. Bunch *et al.*, *Nano Lett.* **8**, 2458 (2008).
2. O. Leenaerts, B. Partoens, F. M. Peeters, *Appl. Phys. Lett.* **93**, 193107 (2008).
3. A. K. Geim, *Science* **324**, 1530 (2009).
4. D. A. Dikin *et al.*, *Nature* **448**, 457 (2007).
5. G. Eda, M. Chhowalla, *Adv. Mater.* **22**, 2392 (2010).
6. J. T. Robinson *et al.*, *Nano Lett.* **8**, 3441 (2008).
7. See supporting material on *Science* Online.
8. F. J. Norton, *J. Am. Ceram. Soc.* **36**, 90 (1953).
9. M. J. McAllister *et al.*, *Chem. Mater.* **19**, 4396 (2007).
10. H. K. Jeong *et al.*, *Chem. Phys. Lett.* **470**, 255 (2009).
11. A. Lerf *et al.*, *J. Phys. Chem. Solids* **67**, 1106 (2006).
12. S. Cerveny, F. Barros-Bujans, Á. Alegría, J. Colmenero, *J. Phys. Chem. C* **114**, 2604 (2010).
13. N. R. Wilson *et al.*, *ACS Nano* **3**, 2547 (2009).
14. D. Pacilé *et al.*, *Carbon* **49**, 966 (2011).
15. R. Zangi, A. E. Mark, *Phys. Rev. Lett.* **91**, 025502 (2003).
16. N. Giovambattista, P. J. Rossky, P. G. Debenedetti, *Phys. Rev. Lett.* **102**, 050603 (2009).
17. J. K. Holt *et al.*, *Science* **312**, 1034 (2006).
18. M. Majumder, N. Chopra, R. Andrews, B. J. Hinds, *Nature* **438**, 44 (2005).
19. X. Peng, J. Jin, Y. Nakamura, T. Ohno, I. Ichinose, *Nat. Nanotechnol.* **4**, 353 (2009).
20. X. Qin, Q. Yuan, Y. Zhao, S. Xie, Z. Liu, *Nano Lett.* **11**, 2173 (2011).
21. M. Whitby, N. Quirke, *Nat. Nanotechnol.* **2**, 87 (2007).
22. J. C. Rasaiah, S. Garde, G. Hummer, *Annu. Rev. Phys. Chem.* **59**, 713 (2008).
23. J. Köfinger, G. Hummer, C. Dellago, *Proc. Natl. Acad. Sci. U.S.A.* **105**, 13218 (2008).
24. J. A. Thomas, A. J. H. McGaughey, *Phys. Rev. Lett.* **102**, 184502 (2009).
25. Y. Li, J. Xu, D. Li, *Microfluid. Nanofluid.* **9**, 1011 (2010).
26. F. Caupin, M. W. Cole, S. Balibar, J. Treiner, *Europhys. Lett.* **82**, 56004 (2008).
27. A. I. Livshits, M. E. Notkin, V. I. Pistunovich, M. Bacal, A. O. Busnyuk, *J. Nucl. Mater.* **220-222**, 259 (1995).
28. N. Goedecke, J. Eijkel, A. Manz, *Lab Chip* **2**, 219 (2002).

Acknowledgments: This work was supported by the Engineering and Physical Research Council (UK), the U.S. Office of Naval Research, the U.S. Air Force Office of Scientific Research, the Royal Society, and the Körber Foundation. We thank K. S. Novoselov, E. Hill, P. Blake, S. Neubeck, and R. Joshi for their help. H.A.W. is grateful for support from the National Science Foundation of China and Oversea Academic Training Funds–University of Science and Technology of China.

Supporting Online Material

www.sciencemag.org/cgi/content/full/335/6067/442/DC1
Materials and Methods
SOM Text
Figs. S1 to S8
References (*29*–*38*)

25 July 2011; accepted 17 November 2011
10.1126/science.1211694

Ultrafast Viscous Permeation of Organic Solvents Through Diamond-Like Carbon Nanosheets

Santanu Karan,[1] Sadaki Samitsu,[1] Xinsheng Peng,[1]* Keiji Kurashima,[1] Izumi Ichinose[1,2]†

Chemical, petrochemical, energy, and environment-related industries strongly require high-performance nanofiltration membranes applicable to organic solvents. To achieve high solvent permeability, filtration membranes must be as thin as possible, while retaining mechanical strength and solvent resistance. Here, we report on the preparation of ultrathin free-standing amorphous carbon membranes with Young's moduli of 90 to 170 gigapascals. The membranes can separate organic dyes at a rate three orders of magnitude greater than that of commercially available membranes. Permeation experiments revealed that the hard carbon layer has hydrophobic pores of ~1 nanometer, which allow the ultrafast viscous permeation of organic solvents through the membrane.

About 40 years ago, reverse-osmosis membranes applicable to seawater desalination were prepared by plasma polymerization of organic monomers (*1*). Membranes obtained from hydrophilic monomers showed high salt rejection and water permeability (*2*, *3*). The permeation mechanism was discussed in terms of the free-volume theory of polymers (*4*, *5*) or the hydrodynamic flow of water through micropores. However, initial expectations for the use of plasma-polymerized membranes gradually diminished with the improved performance of cross-linked polyimide membranes (*6*). Today, asymmetric polyimide membranes are mass-produced for organic solvent nanofiltration by the phase-inversion method. Meanwhile, thin supported carbon membranes made by various techniques are mainly used for gas separations (*7*, *8*).

Diamond-like carbon (DLC) was also made ~40 years ago by Aisenberg and Chabot (*9*). They prepared thin transparent films very similar to diamond by means of an ion-beam deposition technique. Currently, a widely used technique for DLC deposition is plasma chemical vapor deposition using organic compounds (*10*, *11*). In plasma polymerization of organic compounds, a highly cross-linked network of sp^3 carbons is obtained under certain conditions, which provides the resulting thin carbon films with mechanical stability broadly comparable to diamond. We have become interested in the process by which molecules permeate through such a highly cross-linked molecular network. By improving the permeability, we can thereby obtain extremely hard and thin carbon membranes with great advantages for separation technologies.

We demonstrate the ultrafast permeation of organic solvents through DLC nanosheets, free-standing amorphous carbon membranes with thicknesses ranging from 10 to 40 nm. In addition to their high permeability for various solvents, the membranes have excellent separation performance for organic solutes. Interestingly, the solvent flux was mainly affected by the viscosity of the solvents, not by their molecular size or dipole moment.

We prepared the uniform ultrathin DLC membrane on a sacrificial layer of cadmium hydroxide nanostrands (*12*) by using a parallel-plate plasma-enhanced chemical vapor deposition reactor [radio frequency (RF) power: 5 to 50 W at 13.56 MHz, deposition time: 10 to 370 s, pressure: 1 to 6 Pa] (figs. S1 to S3). To prevent damage of the nanostrands, the substrate temperature was maintained at –20°C. We carefully removed the sacrificial layer by treating it with an ethanolic solution of hydrochloric acid (Fig. 1, C to F). The configuration of the filtration membrane is shown in Fig. 1A. In this case, a 35-nm DLC membrane is formed on a 200-nm-pore alumina support. The membrane has a relatively porous layer of thickness ~10 nm where removal of the nanostrands occurred. However, the overall membrane was completely defect-free, as observed by scanning electron microscopy (SEM), and could be used for high-pressure filtration up to at least 2.0 MPa. Nano-indentation measurements confirmed that the membrane prepared from acetylene diluted in argon gas (RF power: 50 W) has a Young's modulus of 170 GPa and a hardness of 20.1 GPa (Table 1). In this case, the Young's modulus is one-seventh the elastic modulus of diamond (1050 to 1200 GPa) (*13*). Solid-state ^{13}C cross-polarization/magic angle spinning nuclear magnetic resonance (CP/MAS NMR) measurements revealed that the membrane contains 47% sp^3 carbons and 53% sp^2 carbons (fig. S4) (*14*). High-resolution transmission electron microscopy (HRTEM) observations confirmed that the acetylene membrane produced at a low substrate temperature (–20°C) was a typical hydrogenated amorphous carbon (a-C:H soft) (fig. S5) (*15*). Fourier-transform infrared measurements indicated the membrane has a relatively high hydrogen content (fig. S6). Furthermore, we estimated the carbon content to be 95.6 atomic % by x-ray photoelectron spectroscopy (XPS) (fig. S7 and table S1). Deconvolution of the C_{1S} spectra indicated that some of the carbon atoms had been oxidized to form ether (or alcohol), carbonyl, and ester (or carboxyl) groups. Based on these data, the internal chemical structure of the acetylene membrane is presumed to be as shown in Fig. 1B.

DLC membranes made from pyridine and hexamethyldisiloxane (HMDS) gave high elastic moduli of 106 and 91.8 GPa, respectively, and

[1]Polymer Materials Unit, National Institute for Materials Science, 1-1 Namiki, Tsukuba, Ibaraki 305-0044, Japan. [2]Japan Science and Technology Agency (JST), Core Research for Evolutional Science and Technology (CREST), 5 Sanbancho, Chiyoda-ku, Tokyo 102-0075, Japan.

*Present address: Department of Materials Science and Engineering, Zhejiang University, Hangzhou 310027, China.
†To whom correspondence should be addressed. E-mail: ichinose.izumi@nims.go.jp

had significant nitrogen or silicon content (Table 1 and figs. S8 and S9). The density of the membranes was in the range of 1.96 to 2.45 g/cm^3, which was generally higher than the value for general amorphous carbon (1.6 to 2.2 g/cm^3) (fig. S6) (*10*, *16*). These results indicate that dense, three-dimensional network structures are formed by considerable carbonization of the precursor monomers. Roughly speaking, our DLC membranes have elastic moduli ~50 times greater than the values for high-strength engineering plastics and ~10 times less than the value for diamond.

For the DLC membranes, we investigated the permeation properties of various organic solvents. In Fig. 2A, the fluxes of different solvents at a pressure difference of 80 kPa are plotted along with their viscosities. In the case of the 35-nm-thick acetylene membrane, hexane, with the smallest viscosity of 0.31 centipoise (cP), gave a surprisingly high flux of 382.9 liters per square meter·hour (L/m^{2}h). Acetonitrile (0.35 cP) gave the second highest value of 235.2 L/m^{2}h. In contrast, the relatively viscous liquid 1-butanol (2.95 cP) gave the lowest flux (27.8 L/m^{2}h). Thus, the solvent permeability increased in inverse proportion to the viscosity. The fluxes of chloroform, ethanol, and benzene also showed the same tendency (fig. S10 and table S2). The solvent polarity did not affect the permeation, at least in the range between acetonitrile and hexane. This is probably because the interaction from a hydrophobic pore is nonspecific to solvents. The HMDS membrane showed a similar inverse proportionality between solvent flux and viscosity (blue curve in Fig. 2A). In both cases, small deviations were observed only for methanol and toluene. The relatively bulky toluene had a flux around two-thirds that of methanol, despite having a slightly lower viscosity. It is apparent that these DLC membranes allow for fast permeation of organic solvents. The apparent viscosity dependence indicates that the hard network structure does not swell in the presence of these solvents. In fact, we confirmed that solvent flux does not change with time (fig. S11). For membranes with many pores of a few nanometers in size, viscous flow can be readily explained by the Hagen-Poiseuille (HP) equation (*17*, *18*)

$$J = \varepsilon\pi r_p^2 \Delta p/\delta\mu\delta\tau \quad (1)$$

Indeed, we observed that the flux (J) increases linearly with applied pressure (Δp), at least in the range 0.08 to 2.0 MPa (fig. S10) (ε, surface porosity; r_p, pore radius; μ, viscosity; δ, membrane thickness; τ, tortuosity). The diffusive transport of solvents that is usually seen in dense polymer membranes and generally gives very low solvent flux (*19*) does not occur with these DLC membranes. However, these membranes do not have any large pores to allow permeation of the solvents as a continuum flow. As confirmed by HRTEM observations, the pore size seems to be no more than 1 nm (fig. S5).

Figure 2B shows the filtration performance of an acetylene membrane for protoporphyrin-IX (PPh-IX) [molecular weight (MW): 562.7]. The membrane could completely reject the protoporphyrin with a molecular width of 1.47 nm (fig. S12), indicating that there are no pores larger than 1.4 nm. The membrane could also reject 99.8% of a fluorescent dye (MW: 389.4) with a width of 1.28 nm, and it rejected azobenzene (MW: 182.2), a small dye molecule with a width of 0.69 nm, to 93.3%. The rejection performance was very constant with time (fig. S13). As mentioned above, our acetylene membrane allows very fast permeation of toluene. However, azobenzene, with the same width and double the length of toluene, cannot permeate through the membrane. This is probably due to the tortuous structure of the solvent pathway through the ultrathin DLC membrane. Although we cannot necessarily assume that the solvents permeate as a continuum flow, it is important that we can analyze the flux in terms of the HP equation. That is, the viscosity-flux and pressure-flux dependencies strongly indicate that the HP equation is extendable to molecular-sized pores. From the rejection of azobenzene (94.4%), the pore size seems to be somewhat larger than the width (*20*, *21*). Supposing a pore size of 1.0 nm, we calculated the surface porosity (ε) of a 35-nm-thick acetylene membrane (RF power: 10 W) to be 12.4%, where an ethanol flux of 67.3 L/m^{2}h at a pressure difference (Δp) of 80 kPa, a viscosity (μ) of 1.19 × 10^{-3} Pa·s (1.19 cP) at 20°C, and a tortuosity (τ) of 1.25 were used for the calculation (*17*) (note that the viscosity and tortuosity have some uncertainty). The actual membrane would have a distribution of pore sizes. The blue circles in Fig. 1B represent a surface porosity of ~12% in area. Judging from the observed density of 2.45 g/cm^3, the nonpore regions are expected to be filled with dense hydrogenated amorphous carbon. The applicability of the HP equation to our membranes needs to be verified, because the molecular sizes of organic solvents are close to or no less than one-third the size of the pores in the membranes.

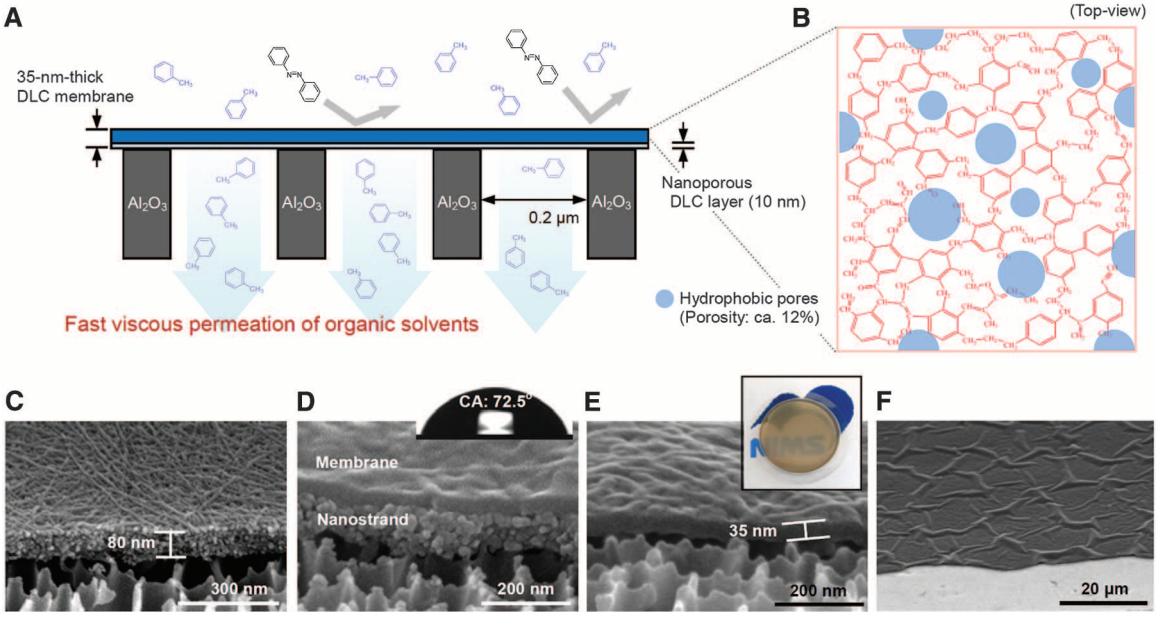

Fig. 1. (**A**) Schematic presentation of a free-standing DLC membrane formed on submicron pores of a porous alumina support. (**B**) Internal structure of the membrane inferred from ^{13}C CP/MAS NMR and XPS. Chemical structures are drawn at a magnification of 1.5, as compared with the hydrophobic pores. (**C** to **E**) Cross-sectional SEM images of a sacrificial 80-nm-thick nanostrand layer on a porous alumina support, a carbon layer deposited on the nanostrand layer, and 35-nm-thick DLC membrane obtained after removal of the nanostrands with HCl. (**F**) Low-magnification SEM image of (E). These images were taken after applying a 3-nm platinum coating. Inset in (D) shows a photographic image of a water droplet on the deposited DLC membrane (CA, contact angle). Inset in (E) shows the DLC membrane formed on a 25-mm porous alumina support.

However, it should be possible to say that our DLC membranes have an abundance of pores that are equivalent to ~12% porosity in the HP equation.

Table 2 summarizes the filtration performance of DLC membranes prepared from various precursor gases (monomers). In preparation at a substrate temperature of –20°C, methane gave membranes with pores of a few nanometers. The rejection values for azobenzene and a fluorescein derivative [fluorescein-4-isothiocyanate (FI)] were 23.0 and 41.3%, respectively. The allylamine membrane also gave low rejection values for these molecules. On the other hand, acetylene and pyridine gave rejection values of more than 90% for azobenzene. In a comparison of the three acetylene membranes, the membrane deposited at an RF power of 10 W gave the highest flux for ethanol and also the highest rejection value for azobenzene. The low RF power probably acts to help prevent complete carbonization of the growing DLC layer and to give a highly microporous structure. We confirmed that the performance of the DLC membranes varies widely with the preparation parameters. This indicates that there are many ways to design cross-linked network structures in DLC membranes in addition to controlling the composition and hydrophobicity. It is also important to stress that the filtration performance changes substantially with the membrane thickness. For example, a 10-nm-thick acetylene membrane allows hexane permeation at a flux of 2911 L/m^{2}h at a pressure difference of 80 kPa and completely rejects 5-nm gold nanoparticles from an ethanolic solution (fig. S14 and table S3). This membrane thus offers an innovative ultrafiltration membrane for organic solvents. The observed flux is overwhelmingly higher than those of other known ultrafiltration membranes with similar rejection properties.

More importantly, the ethanol flux through one of the 35-nm-thick acetylene membranes (67.3 L/m^{2}h) is about three orders of magnitude greater than those of commercially available organic solvent nanofiltration membranes [see supporting online material (SOM)]. This DLC membrane has an extremely sharp molecular weight cut-off, as indicated by a rejection value for azobenzene of more than 94% (Table 2 and fig. S15). From the viewpoint of applications in the chemical and petrochemical industries (*19*, *22*), the ultrafast permeation of organic sol-

Table 1. Composition and mechanical properties of acetylene, pyridine, and HMDS membranes. ND, not determined.

Monomers	Membrane atomic composition*					Density† (g/cm^3)	Young's modulus‡ (GPa)	Hardness‡ (GPa)
	C	N	O	Si	Ar			
Acetylene	95.6	ND	3.8	ND	0.6	2.45	170	20.1
Pyridine	87.8	7.9	4.3	ND	ND	2.08	106	12.3
HMDS	49.9	ND	20.7	29.4	ND	1.96	91.8	10.1

*DLC membranes were prepared at RF power of 50 W using 20% acetylene/Ar gas at 5 Pa, pyridine at 2 Pa, and HMDS at 1.5 Pa. The atomic composition was estimated by XPS measurements. †Density was estimated by a quartz crystal microbalance technique for 40- to 80-nm-thick membranes. ‡Young's modulus and hardness were measured by a nano-indentation technique for ~300-nm-thick membranes deposited on silicon wafers.

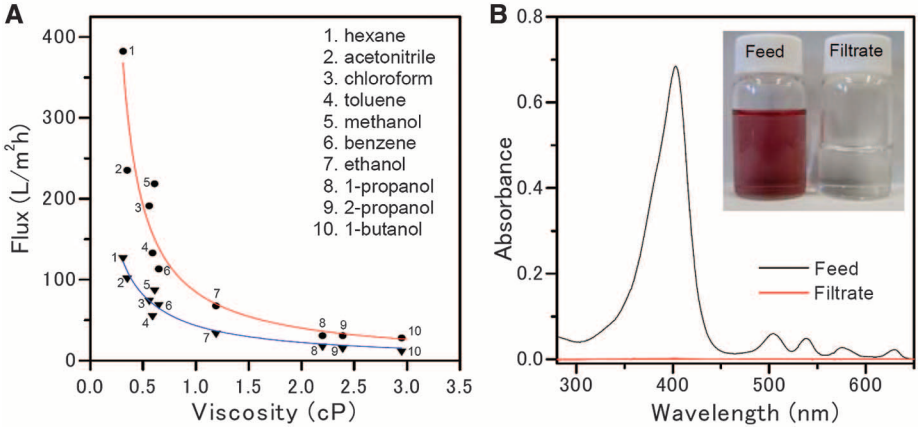

Fig. 2. (**A**) Relation between flux and viscosity of organic solvents showing inverse proportionality. Red curve, fit of fluxes of different solvents passed though a 35-nm-thick acetylene membrane deposited at 10 W; blue curve, fit of fluxes of different solvents though a 35-nm-thick HMDS membrane deposited at 50 W. The experiments were conducted at 20°C at 80 kPa. Note that the flux values were calculated for the membrane area covering the pores of the alumina support (porosity: 50%). (**B**) Ultraviolet-visible absorption spectra of PPh-IX ethanolic solution (0.05 mM) before and after filtration through a 35-nm-thick acetylene membrane (30 W). (Inset) Photograph of the feed and filtrate of the PPh-IX solution.

Table 2. Filtration performance of free-standing DLC membranes.

Monomer*	RF power (W)	Pressure (Pa)	Thickness (nm)	Contact angle (deg)	Ethanol flux† (L/m^{2}h)	AB‡ (0.69 nm)		FI‡ (1.28 nm)		PPh-IX‡ (1.47 nm)	
						Flux (L/m^{2}h)	Rejection (%)	Flux (L/m^{2}h)	Rejection (%)	Flux (L/m^{2}h)	Rejection (%)
Methane	10	5.0	35 ± 3	73.2 ± 2.1	201.1	188.8	23.0	179.8	41.3	129.7	81.5
Butadiene	20	5.0	35 ± 3	66.2 ± 1.4	45.8	35.9	86.6	32.3	99.3	25.5	100
Acetylene	10	5.0	35 ± 3	72.5 ± 1.1	67.3	51.5	94.4	47.8	99.6	44.6	100
Acetylene	30	5.0	36 ± 2	71.1 ± 1.2	54.4	40.2	93.3	32.7	99.8	31.1	100
Acetylene	50	5.0	35 ± 4	70.0 ± 1.4	21.0	10.3	87.2	7.5	100	7.2	100
Pyridine	50	2.0	35 ± 5	61.0 ± 1.1	37.8	32.1	92.7	21.4	99.8	18.9	100
HMDS	50	1.5	36 ± 4	93.8 ± 1.7	34.0	25.5	79.9	21.5	98.5	16.9	99.6
ATMS	50	1.5	36 ± 4	66.0 ± 0.8	38.2	35.2	85.7	31.8	99.6	19.4	100
Propylamine	10	5.0	40 ± 2	71.2 ± 0.6	24.3	20.1	87.0	15.2	99.8	12.5	100
Allylamine	20	6.0	50 ± 4	62.6 ± 1.4	25.5	16.9	48.2	10.2	60.9	3.9	99.3

*Butadiene and acetylene gases were introduced after diluting to 20% with Ar. ATMS, allyltrimethoxysilane. Monomer flow rates were 2.71 standard cubic centimeters per minute (sccm) for methane, 1.68 sccm for butadiene, 1.67 sccm for acetylene, and 1.40 sccm for HMDS and ATMS. †The valid area of the free-standing DLC membranes was 0.39 cm^2. ‡AB, azobenzene (0.5 mM in ethanol); FI, fluorescein-4-isothiocyanate (0.05 mM in ethanol); and PPh-IX, protoporphyrin-IX (0.05 mM in ethanol). A permeated volume of no less than 2 ml was collected to determine the rejection value. All the filtration experiments were conducted at 20°C at a pressure difference of 80 kPa.

vents contributes appreciably to improved energy efficiency in recovery of the solvents. A range of industries—including polymer synthesis (*23*), production of biofuels (*24*), environmental remediation (*25*), and oil extraction in the food industry (*19*)—have a strong demand for solvent-resistant nanofiltration membranes with superior permeability characteristics. For these purposes, nanoporous free-standing sheets of carbon nanotubes (*26*, *27*) and other inorganic membranes (*28*) have been studied globally. However, it has been a challenge to produce such membranes in an industrially applicable process. DLC membranes have been found to be extremely dense and suitable for use in gas barrier applications (*29*, *30*). In this Report, we demonstrate that DLC membranes can be prepared with extremely high solvent permeability while maintaining considerable mechanical strength.

References and Notes

1. K. R. Buck, V. K. Davar, *Br. Polym. J.* **2**, 238 (1970).
2. J. R. Hollahan, T. Wydeven, *Science* **179**, 500 (1973).
3. H. Yasuda, C. E. Lamaze, *J. Appl. Polym. Sci.* **17**, 201 (1973).
4. A. A. Bondi, *Physical Properties of Molecular Crystals, Liquids, and Glasses* (Wiley, New York, 1968).
5. D. W. Van Krevelen, *Properties of Polymers* (Elsevier, Amsterdam, 1990).
6. Y. H. See Toh, F. W. Lim, A. G. Livingston, *J. Membr. Sci.* **301**, 3 (2007).
7. M. Kiyono, P. J. Williams, W. J. Koros, *J. Membr. Sci.* **359**, 2 (2010).
8. A. F. Ismail, D. Rana, T. Matsuura, H. C. Foley, *Carbon-Based Membranes for Separation Processes* (Springer, New York, 2011).
9. S. Aisenberg, R. Chabot, *J. Appl. Phys.* **42**, 2953 (1971).
10. J. Robertson, *Mater. Sci. Eng. Rep.* **37**, 129 (2002).
11. X. D. Pan, E. A. Maydell, R. H. Milne, D. J. Fabian, *Vacuum* **41**, 1360 (1990).
12. I. Ichinose, K. Kurashima, T. Kunitake, *J. Am. Chem. Soc.* **126**, 7162 (2004).
13. M. Werner, S. Hein, E. Obermeier, *Diamond Relat. Mater.* **2**, 939 (1993).
14. We used the term of DLC to emphasize the mechanical stability of the membranes. However, the fraction of sp^2 carbon is relatively high and is close to that in disordered carbon (see SOM).
15. P. Koidl, Ch. Wild, B. Dischler, J. Wagner, M. Ramsteiner, *Mater. Sci. Forum* **52-53**, 41 (1990).
16. P. J. R. Honeybone, R. J. Newport, J. K. Walters, W. S. Howells, J. Tomkinson, *Phys. Rev. B* **50**, 839 (1994).
17. K. Li, *Ceramic Membranes for Separation and Reaction* (Wiley, West Sussex, UK, 2007).
18. Q. Zhang, S. Ghosh, S. Samitsu, X. Peng, I. Ichinose, *J. Mater. Chem.* **21**, 1684 (2011).
19. P. Silva, L. G. Peeva, A. G. Livingston, in *Advanced Membrane Technology and Applications*, N. N. Li, A. G. Fane, W. S. W. Ho, T. Matsuura, Eds. (Wiley, Hoboken, NJ, 2008), pp. 451–467.
20. J. L. Anderson, J. A. Quinn, *Biophys. J.* **14**, 130 (1974).
21. G. F. Froment, K. B. Bischoff, *Chemical Reactor Analysis and Design* (Wiley, New York, 1979).
22. P. Vandezande, L. E. M. Gevers, I. F. J. Vankelecom, *Chem. Soc. Rev.* **37**, 365 (2008).
23. S. So, L. G. Peeva, E. W. Tate, R. J. Leatherbarrow, A. G. Livingston, *Org. Process Res. Dev.* **14**, 1313 (2010).
24. R. Othman, A. W. Mohammad, M. Ismail, J. Salimon, *J. Membr. Sci.* **348**, 287 (2010).
25. I. C. Escobar, S. Hong, A. Randall, *J. Membr. Sci.* **175**, 1 (2000).
26. J. K. Holt *et al.*, *Science* **312**, 1034 (2006).
27. F. Fornasiero *et al.*, *Proc. Natl. Acad. Sci. U.S.A.* **105**, 17250 (2008).
28. C. C. Striemer, T. R. Gaborski, J. L. McGrath, P. M. Fauchet, *Nature* **445**, 749 (2007).
29. A. Shirakura *et al.*, *Thin Solid Films* **494**, 84 (2006).
30. G. A. Abbas, S. S. Roy, P. Papakonstantinou, J. A. McLaughlin, *Carbon* **43**, 303 (2005).

Acknowledgments: We gratefully acknowledge financial support from JST, CREST, and a grant-in-aid for scientific research from the Ministry of Education, Culture, Sports, Science and Technology, Japan (no. 23350105). A part of this Report was used for a Japanese patent [application no. (2010) 180194].

Supporting Online Material

www.sciencemag.org/cgi/content/full/335/6067/444/DC1
Materials and Methods
Figs. S1 to S15
Tables S1 to S3
References (*31*–*55*)

2 August 2011; accepted 7 November 2011
10.1126/science.1212101

An All-Silicon Passive Optical Diode

Li Fan,[1,2]* Jian Wang,[1,2]* Leo T. Varghese,[1,2]* Hao Shen,[1,2] Ben Niu,[1,2] Yi Xuan,[1,2] Andrew M. Weiner,[1,2] Minghao Qi[1,2,3]†

A passive optical diode effect would be useful for on-chip optical information processing but has been difficult to achieve. Using a method based on optical nonlinearity, we demonstrate a forward-backward transmission ratio of up to 28 decibels within telecommunication wavelengths. Our device, which uses two silicon rings 5 micrometers in radius, is passive yet maintains optical nonreciprocity for a broad range of input power levels, and it performs equally well even if the backward input power is higher than the forward input. The silicon optical diode is ultracompact and is compatible with current complementary metal-oxide semiconductor processing.

Nonreciprocal transmission is fundamental to information processing. Electrical nonreciprocity, or the diode effect, had been realized in integrated form with a semiconductor p-n junction. Optical nonreciprocity (ONR) is inherently difficult because of the time-reversal symmetry of light-matter interaction (*1*). Previously reported observations of ONR were based on the magneto-optic effect (*2*–*4*), optical nonlinearity (*5*–*8*), electro-absorption modulation (*9*), cholesteric liquid crystals (*10*), optomechanical cavities (*11*), indirect interband photonic transitions (*12*), and the opto-acoustic effect (*13*). However, complementary metal-oxide semiconductor (CMOS)–compatible passive optical diodes with a footprint and functionality analogous to those of p-n junctions have not been realized at the near-infrared wavelengths that are preferred for silicon (Si) photonics.

Our optical diode (Fig. 1A) is based on strong optical nonlinearity in high–quality factor (Q) Si microrings (*14*–*17*). It consists of a high-Q all-pass notch filter (NF) operating near the critical coupling regime (*17*) (Fig. 1B) and an add-drop filter (ADF) (*14*, *16*, *18*) with asymmetric power coupling to the bus waveguides (Fig. 1C). The resonant wavelength of the NF is thermally tuned to match that of the ADF through the thermo-optic effect of silicon (*19*).

A microring accumulates optical energy at its resonant wavelength. The schematics in Fig. 1, E and F, show that light couples into the microring in the ADF through two different gaps, G_2 and G_3. If we define forward and backward input power as $P_{c,f}$ and $P_{in,b}$, respectively, the optical energy stored in the microring near its resonant wavelength, λ_{ADF}, can be expressed as

$$U_{forward}(\lambda) = \frac{P_{c,f}}{Q_{G_2}} Q_{ADF}^2 K(\lambda) \qquad (1)$$

and

$$U_{backward}(\lambda) = \frac{P_{in,b}}{Q_{G_3}} Q_{ADF}^2 K(\lambda) \qquad (2)$$

where Q_{ADF} is the ring's loaded quality factor, Q_{G_2} and Q_{G_3} are power coupling quality factors that are exponentially proportional to the gap sizes, and $K(\lambda)$ represents all other terms that are independent of propagation direction for a linear system (*14*).

The energy enhancement factor in the ring depends on the propagation direction because of our asymmetric design ($Q_{G_2} \approx 300{,}000$, $Q_{G_3} \approx 192{,}000$, and $Q_{ADF} \approx 43{,}800$, all through curve-fitting), and $(U_{forward}/U_{backward}) = (Q_{G_3}/Q_{G_2}) = 0.64$ for $P_{c,f} = P_{in,b}$. With high input power at $\lambda_0 = \lambda_{ADF}$, the power density inside the ring will be amplified substantially because of its high Q factors and small radius; this induces optical nonlinearity in silicon (*20*–*23*) and a red shift in the ring's resonance ($\lambda'_{ADF} > \lambda_0$, Fig. 1F). Because less energy is stored in the ring during forward

[1]Birck Nanotechnology Center, Purdue University, West Lafayette, IN 47907, USA. [2]School of Electrical and Computer Engineering, Purdue University, West Lafayette, IN 47907, USA. [3]Shanghai Institute of Microsystem and Information Technology, Chinese Academy of Sciences, Shanghai 20050, China.

*These authors contributed equally to this work.
†To whom correspondence should be addressed. E-mail: mqi@purdue.edu